analytical chemistry

Article

Cite This: Anal. Chem. 2018, 90, 1652−1659

pubs.acs.org/ac

Study of Oscillating Electroosmotic Flows with High Temporal and Spatial Resolution

Wei Zhao,[†,‡] Xin Liu,[‡] Fang Yang,[§] Kaige Wang,[†] Jintao Bai,[†] Rui Qiao,*[,∥] and Guiren Wang*[,‡]

[†]Institute of Photonics and Photon-technology, International Scientific and Technological Cooperation Base of Photoelectric Technology and Functional Materials and Application, Northwest University, 229 North Taibai Road, Xi'an 710069, People's Republic of China

[‡]Department of Mechanical Engineering & Biomedical Engineering Program, University of South Carolina, Columbia, South Carolina 29208, United States

[§]Key Laboratory for Molecular Enzymology and Engineering of Ministry of Education, Jilin University, Changchun 130012, People's Republic of China

[∥]Department of Mechanical Engineering, Virginia Tech, Blacksburg, Virginia 24061, United States

Supporting Information

ABSTRACT: Near-wall velocity of oscillating electroosmotic flow (OEOF) driven by an AC electric field has been investigated using a laser-induced fluorescence photobleaching anemometer (LIFPA). For the first time, an up to 3 kHz velocity response of OEOF has been successfully measured experimentally, even though the oscillating velocity is as low as 600 nm/s. It is found that the oscillating velocity decays with the forcing frequency f_f as $f_f^{-0.66}$. In the investigated range of electric field intensity (E_A), below 1 kHz, the linear relation between oscillating velocity and E_A is also observed. Because the oscillating velocity at high frequency is very small, the contribution of noise to velocity measurement is significant, and it is discussed in this manuscript. The investigation reveals the instantaneous response of OEOF to the temporal change of electric fields, which exists in almost all AC electrokinetic flows. Furthermore, the experimental observations are important for designing OEOF-based micro/nanofluidics systems.

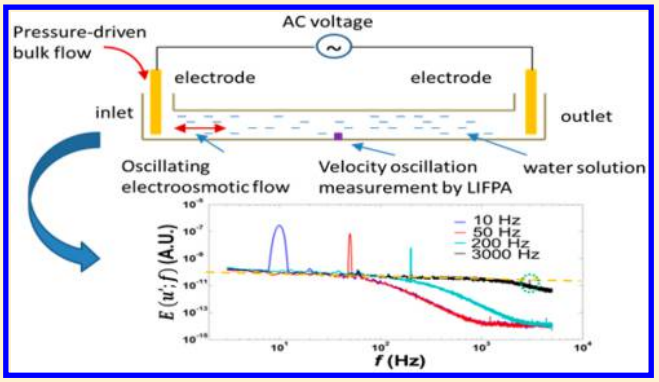

In micro- and nanofluidic systems, due to the large surface-to-volume ratio, electroosmotic flow (EOF) has been widely used to pump fluids and manipulate objects for various applications, such as DNA transport, hybridization and separation in biomedical engineering, and enhancing heat and mass transfer.[1−5]

At the early stages, most of the investigations focused on the EOF driven by direct current (DC). The relevant devices have been proven to be effective in driving flows in micro/nanochannels, which are further used to transport DNA, protein, and cells. However, when the length of channels is long, it normally requires high voltage to generate sufficiently strong electric field to drive the flow. This leads to several drawbacks, such as gas bubble formation due to electrolysis and excessive heating due to electrothermal effects.

Relative to DC EOF, the EOF generated by AC electric fields (i.e., AC EOF) has attracted wide interest in the past decade. Compared to DC EOF, AC EOF-based micropumps require lower voltage to pump fluids. This can avoid the generation of microbubbles and make the devices portable.

In microfluidics, as early as in 2000, Green et al.[6] reported AC EOF (also known as induced-charge electroosmotic flow, ICEOF) near planar microelectrodes. By monitoring latex tracer particles, the velocity of the flow is experimentally investigated and exhibits apparent dependency on the frequency of the AC field. On the basis of AC EOF, Studer et al.[7] designed a micropump for tunable flow control. Under very low voltages (below 10 V, rms value), a maximum flow speed of 500 μm/s can be achieved at AC electric field of tens of kHz. In the same year, Debesset et al.[8] also designed a micropump for chromatographic application, by using AC EOF. A maximum speed of 50 μm/s was realized. Although the flow speed was an order smaller than that observed by Studer et al.,[7] they successfully found that in the investigated parametric region, the flow speed of micropump had approximately linear relation with applied AC voltage and frequency. Later, in 2005, Gagnon and Chang[9] combined an AC EOF with a dielectrophoretic (DEP) flow to achieve fast bacteria detection. The bulk flow velocity due to the AC EOF could be up to 1000

Received: July 27, 2017
Accepted: December 19, 2017
Published: December 19, 2017

DOI: 10.1021/acs.analchem.7b02985
Anal. Chem. 2018, 90, 1652−1659

μm/s. Ramos et al.[10] also suggested a low voltage AC EOF by applying a traveling wave scheme. Although the flow speed was only ~100 μm/s, they observed an interesting reversal flow in which the flow direction could vary with applied AC voltage. In practical applications, EOF with low speed is not necessarily a drawback. For instance, in DNA characterization, high flow velocity is not desired, because the fast translocation of DNA molecule in micro- and nanochannels makes the interpretation of the current signal difficult. Bown and Meinhart[11] developed a DNA concentrator by using AC EOF, and a concentration factor of 8 was achieved. Also, AC EOF was used to induce large-scale secondary circular flows and enhance mixing, as have been demonstrated by Ng et al.[12] There are also many other experimental works related to AC EOF.[13−18] However, all of them focused on the mean or bulk velocity of fluids, not the instant flow response to AC electric fields, which could be more complicated.

Recently, most of the studies on the instantaneous velocity of AC EOF are from analytical solutions or numerical simulations. Based on linear and thin electric double layer (EDL) approximation, González et al.[19] theoretically investigated the AC EOF which was experimentally studied by Green et al.[6] The relation between the AC frequency and the AC EOF velocity was clarified. Later, Dutta and Beskok[20] systematically investigated the analytical solutions of an oscillating electro-osmotic flow (OEOF) by analogy to Stoke's second problem, in a parallel plate microchannel, where an AC electric field is applied. They solved Poisson−Boltzmann and Navier−Stokes equations with no-slip boundary conditions. Relying on the assumption that the ζ-potential was independent of the externally applied electric field and the viscosity of the fluid was constant, analytical solutions had been obtained. Then, Kang et al.[21] solved the OEOF in a circular microchannel by Green's function. Later, Yang et al.[22] and Bhattacharyya et al.[23] obtained the analytical solutions in rectangular and circular microchannels respectively, with the presence of a pressure-driven flow. All the aforementioned investigations are mainly based on 1D and/or linearized models. A remarkable exception are the works by Bazant and his colleagues, in which they first suggested a design of a 3D AC EOF pump[24] and advanced the principle for designing AC EOF pumps.[25] In 2010, they further predicted the nonlinear response under a strong AC electric field.[26] Later, Aboelkassem[27] numerically show that complex flow patterns could also be realized in EOF with sinusoidal surface charges. Recently, the investigations on OEOF turn to viscoelastic fluids[28−31] and nonsinusoidal AC electric fields.[32] In addition, numerical simulation provides another effective way to elucidate the response of OEOF. For example, Lin and Chen[33] utilized Lattice Poisson−Boltzmann method to investigate the OEOF in a parallel plate microchannel with the presence of pressure-driven flow. Besides the aforementioned works, there are still many other theoretical and numerical studies related to OEOF in micro- and nanofluidics applications.[1,17,34−42]

So far, compared to the fruitful investigations from theory and numerical simulations, few experimental researches on the velocity fields of OEOF have been done to help validate the theories and simulations. In fact, even in the limited experimental investigations on the velocity of OEOF, discrepancies between experiments and theories exist.[43] For instance, theories have overpredicted averaged bulk flow,[44] relative to experimental observations.

One of the major obstacles of studying AC EOFs is the lack of reliable flow diagnostic techniques with sufficiently high spatial and temporal resolutions. To the best of the authors' knowledge, almost all the velocity measurement in AC EOFs relies on particles as flow tracers, such as the currently standard velocimeter—micro particle image velocimetry (μPIV). However, as stated by Minor et al.,[45] "a colloidal particle responds much faster to an applied electric field than does the liquid inside the capillary". In fact, for many microflows, particles have different velocities from their surrounding fluids. In a highly disturbed flow, the well-known particle lagging makes it difficult to measure strong velocity fluctuation with high frequency. Since most particles may have more or less charges, erroneous velocity due to electrostatic force cannot be avoided, not only in the presence of EK but also in flows without EK when particles are close to the charged wall.[46] Even for the study of the mean velocity after proper corrections, the theoretical results can still be two orders higher than experimental measurements, as have been shown by Bown and Meinhart.[11] Wu et al.[47] made an attempt to measure a low frequency OEOF by micro-PIV through phase averaging. However, there is no further correction on their measurement to avoid the aforementioned drawbacks of particle-based experimental methods. Due to the limited spatial resolution, this method could not describe OEOF near wall effectively. Most recently, Kneller et al.[48] studied the AC EOF by monitoring the arrival time of a rhodamine B dye. However, the method can only measure the mean rather than the instantaneous velocity.

On the basis of the aforementioned understanding of various electroosmotic flows driven by AC electric field, several different terminologies have been applied to describe the EOF under AC electric field, such as OEOF, ICEOF, and AC EOF. The difference among the definitions is out of the scope of this manuscript. However, all these flows share a common feature; that is, they are partially or completely transient flows in each period of the AC signal, determined by the characteristic time scale of EOFs and the relaxation time of EDL. Therefore, a detailed investigation on the instantaneous velocity in a typical transient flow is especially important in practical applications.

In this investigation, we study a typical transient flow (i.e., OEOF) to show how its flow velocity responds to the external AC electric field instantaneously. For this purpose, the laser-induced fluorescence photobleaching anemometer (LIFPA) developed recently[49−53] is used to study the velocity evolution of OEOF. LIFPA uses electrically neutral and small molecule dye as an idea flow tracer, which can impartially reflect the flow velocity in electrokinetics. In previous investigations, LIFPA has shown simultaneously ultrahigh spatial (~200 nm) and temporal (~10 μs) resolutions, and it has been successfully used to detect the rise time of DC EOF[54] and characterize the microelectrokinetic turbulence.[49,50] These features satisfy the requirements of measuring OEOF in the near wall region.

Similar to hot-wire anemometers, the current LIFPA method cannot distinguish velocity directions. Thus, LIFPA is ideally suitable for flows without backflow. For this reason, applying an overlapped bias mean flow velocity could be helpful to increase the temporal resolution when measuring instant flows velocity, as discussed later. Besides, LIFPA's temporal resolution also relies on the mean velocity of oscillating flow, where smaller mean velocity could result in lower temporal resolution of LIFPA. Therefore, a pressure-driven basic flow is used to provide sufficiently large mean flow for the LIFPA measure-

DOI: 10.1021/acs.analchem.7b02985
Anal. Chem. 2018, 90, 1652−1659

ment. Two electrodes are located in the inlet and outlet of a microchannel to apply an approximately uniform electric field. This OEOF could serve as a basic flow for fundamental research of AC EOFs. The oscillating velocity and spectral response are studied in details. The results are compared with analytical solutions. Signal and noise analysis on the LIFPA measurement is also discussed.

EXPERIMENTAL SETUP AND PROCEDURE

Schematic of Microchannel and OEOF. The experimental investigation is carried out in a straight microchannel, which is 5 mm long (l), 200 μm wide (w), and 70 μm high (h), as shown in Figure 1. The microchip is fabricated through

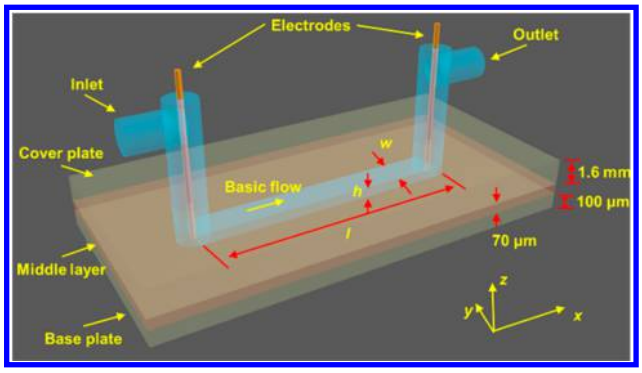

Figure 1. Schematic of the microchannel. x, y, and z represents streamwise, spanwise, and vertical directions, respectively.

layer-by-layer technique,[55] including cover plate, middle layer, and base plate, respectively. The cover and base plates are both assembled by plastic plates. The former is a thick acrylic plate (1.6 mm) with good mechanical strength and transparency. The latter is made by a CLAREX UV transmission filter (ASTRA Products Inc.), which is only 100 μm thick. It has excellent transmission rate for UV light, with durable strength and hard surface. The middle layer is also fabricated by a plastic sheet.

A pressure-driven flow, supplied by a syringe pump (Harvard Apparatus PHD 2000), is used as the basic flow. Two electrodes which are platinum wires with diameter of 127 μm are inserted into the inlet and outlet, respectively, as shown in Figure 1. The high frequency and high accuracy voltages applied on the electrodes are provided by an arbitrary function generator (Tektronix AFG3102). The maximum AC voltage is 20 $V_{p\text{-}p}$ (volts of peak-to-peak), and the equivalent amplitude of the electric field is E_A = 2000 V/m. Because the microchannel is sufficiently long, a quasi-parallel AC electric fields can be generated to drive the EDLs periodically to create OEOF.

In this investigation, as the oscillating velocity of OEOF is small, the requirement for the stability of basic flows is strict. There are two sources of disturbance from basic flows. One is due to the expansion and shrinking of the water supply tubing under high pressure, and the other is caused by the vibration of the water supply tubing. To minimize these influences, PEEK (Polyetheretherketone) tubing is applied to connect the syringe to the inlet of microchannel. Meanwhile, the PEEK tubing is securely fixed by holders to avoid vibration near the inlet.

Aqueous solutions of Coumarin 102 (excited by a 405 nm laser and emitted at 460 nm) with 100 μM concentration are injected into the microchannel by the syringe pump. Because the dye is electrically neutral (Sigma-Aldrich Corp., MO), this small molecule is an idea tracer and can impartially reflect and measure the velocity of OEOF under AC electric field. The dye is first dissolved by methanol and then mixed with DI water. Before LIFPA measurements, the microchannel and PEEK tubing are flushed and rinsed by ethanol first. Then, they are flushed by the 100 μM Coumarin 102 solution. Thus, the residue of solutions and air bubbles can be removed.

Velocity Measured through LIFPA. The principle of LIFPA measurement has been schematically diagrammed in Figure 2. For more details, please refer to the papers of Wang et al.[49,50,52] and Zhao et al.[53] Generally speaking, LIFPA is an optical version of hot-wire anemometers.

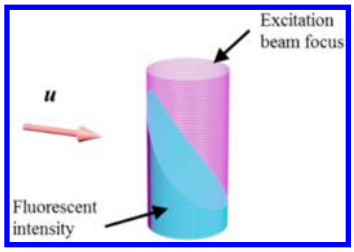

Figure 2. Schematic of the principle of LIFPA measurements.

When a solution of fluorescent dyes with poor photostability flow through the laser focus (as shown by the violet part in Figure 2), because of photobleaching, the efficiency of dyes can be decreased. This leads to a fast decreasing of the local fluorescent intensity (shown by the height of blue part in Figure 2) along the direction of flow velocity u. A faster flow speed has less residence time within the beam and results in a weaker photobleaching. Thus, a higher total fluorescent intensity (i.e., larger volume of the blue part in Figure 2) can be detected by a high sensitivity photo detector. Therefore, a direct relation between flow velocity and the total fluorescent intensity can be established, as plotted in Figure 4. The spatial resolution of LIFPA is determined by the microscopy system (i.e., optical parts). However, the temporal resolution of LIFPA can be influenced by both chemical and dynamical factors, including the frequency (f) of oscillating flow, photobleaching time constant (τ), and the mean velocity of flow. From the investigation of Zhao et al.,[53] for the oscillating velocities at a specific frequency (f) to be measured reliably through LIFPA, it must satisfy the condition below:

$$u_{rms}/U \leq 1/\sqrt{1 + 4\pi^2\tau^2 f^2} \quad (1)$$

In this investigation, the photobleaching time constant τ is about 47 μs.

The LIFPA system is schematically shown in Figure 3. It is developed on the basis of an in-house confocal microscopy system, which is consisted of a 405 nm continuous wave UV laser (50 mW), Olympus PlanApo 100× NA 1.4 oil immersion objective lens and the relevant optical setup. To control the position of the laser focus accurately with sufficiently large displacement, two translation stages are used simultaneously. One is a manual 3D micrometer translation stage (Melles Griot Inc.), and the other is a high-accuracy nanotranslation stage (Physik Instrumente piezo nanocube 3D positioning stage P-611.3SF). The fluorescent signal is captured by a photomultiplier tube (PMT, Hamamatsu R-928). After proper preamplification and electric filtering (Stanford Research SR570 current preamplifer), the voltage signal is recorded on

DOI: 10.1021/acs.analchem.7b02985
Anal. Chem. 2018, 90, 1652−1659

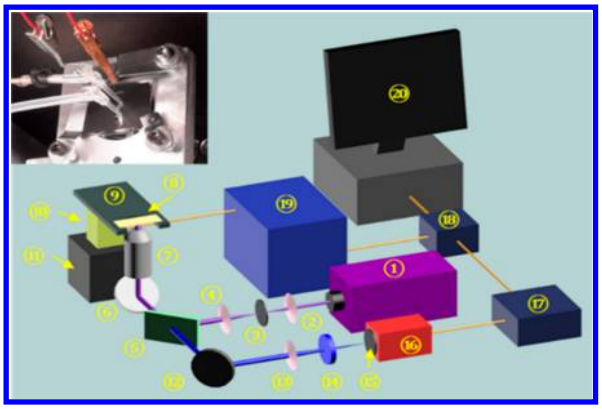

Figure 3. Schematic of the LIFPA system. The system includes: (1) 405 nm CW laser; (2) lens; (3) pinhole; (4) lens; (5) dichroic mirror; (6) mirror; (7) objective lens; (8) microchip; (9) carrier plate; (10) nanometer translation stage; (11) micrometer translation stage; (12) mirror; (13) lens; (14) band-pass filter; (15) pinhole; (16) PMT; (17) current preamplifier and filter (Stanford Research System SR570); (18) A/D convertor; (19) PI nanostage controller; (20) computer. In the inset, it can be seen that, to avoid vibration, the microchip is clamped onto a carrier plate which is fixed on the piezo nano translation stage.

a computer. The control of the nanostage and sampling of fluorescent signal are both through A/D convertor (NI USB-6259) with NI LabVIEW Signal Express software. For details, please refer to the captions of Figure 3. Meanwhile, the actual setup of the microchip can be found in the inset of Figure 3.

In this LIFPA system, the lateral spatial resolution is 203 nm and the axial resolution is around 1 μm.[49] The thickness of the Debye layer ($\lambda = \sqrt{\varepsilon_0\varepsilon_r k_B T/8n_0 e^2 q^2}$, which is only half of the conventional one but is consistent with the one used in the model of Dutta and Beskok[20]) is estimated to be 500 nm, where ε_r = 81 is the dielectric constant of water, ε_0 is the vacuum permittivity, k_B is Boltzmann constant, T is temperature in Kelvin, n_0 is the is the averaged background number of positive or negative ions, e is the elementary charge (C), and q = 1 is the ion valence. The axial resolution of the current LIFPA system is comparable to λ. The LIFPA system could not measure the exact velocity within the AC EDL, but it can provide a reasonable measurement of the outer layer of EDL and can reflect the instantaneous velocity of OEOF. Also, the potential issue that current LIFPA cannot distinguish the flow direction is minimized in this investigation, because the flow is approximately 1D, and the small OEOF cannot induced reverse flow when a pressure-driven flow is present.

LIFPA Calibration. Similar to hot-wire anemometers, LIFPA also needs a calibration between flow velocity and fluorescence intensity, before measuring flow velocity. Here, the velocity calibration of LIFPA is made at the center of the microchannel with a pressure-driven flow. The velocity profile can be described as below:[56,57]

$$U(y,z) = \frac{48Q}{\pi^3 wh}\left\{\sum_{n,\text{odd}}^{\infty}\frac{1}{n^3}\left[1-\frac{\cosh\left(\frac{n\pi y}{h}\right)}{\cosh\left(\frac{n\pi w}{2h}\right)}\right]\sin\left(\frac{n\pi z}{h}\right)\right\}\left[1-\sum_{n,\text{odd}}^{\infty}\frac{192h}{n^5\pi^5 w}\tanh\left(\frac{n\pi w}{2h}\right)\right]^{-1} \quad (2)$$

where U is the local velocity of laminar flow, Q is the flow rate, $-w/2 \le y \le w/2$, $0 \le z \le h$. Given Q, w and h, the velocity at the center of the microchannel, i.e. $U(0,h/2)$ can be easily calculated. Meanwhile, by LIFPA, the total fluorescent intensity—I_f can be measured directly at the corresponding flow velocity. Therefore, $I_f \sim U(0,h/2)$ relation can be subsequently obtained.

The calibration curve of LIFPA is plotted in Figure 4. In the calibration, the current amplifier has a sensitivity of 100 μA/V

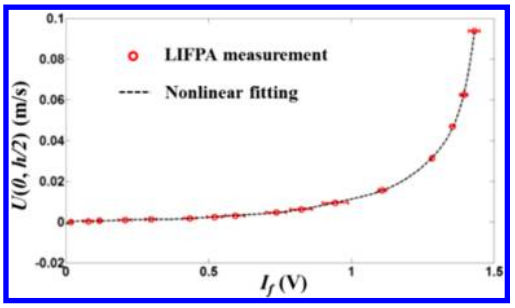

Figure 4. Typical velocity calibration curve measured at the center of microchannel. The velocity is calculated from the flow rate by eq 2. The calibration curve is nonlinearly fitted by polynomial series.

and the threshold value is 100 nA, below which, the signal is considered as noise. A 12 dB low-pass filter with 100 Hz cutoff frequency is adopted to suppress shot noise. It can be seen the data points are well fitted by a 10th order polynomial series. In the low-speed region, the velocity shows good linearity with I_f.

Determine the Position of EDL. To accurately determine the measurement position near the wall, our strategy (as shown in Figure 5) is the following: (1) Generate a low frequency OEOF with sufficiently large oscillating velocity; (2) Move the laser focus from the centerline of microchannel downward and monitor the real-time peak of velocity power spectrum at the forcing frequency; (3) When the peak of the spectrum reaches the maximum value, the corresponding position is considered as the proper position for measuring the velocity of OEOF. In this investigation, the near-wall position for mean and oscillating velocities measurement is z = 2 μm (i.e., 2 μm above the bottom wall).

EXPERIMENTAL RESULTS

Mean Velocity under Different AC Frequency. The mean velocity ($U = \overline{u}$, where u is the instantaneous velocity and the bar represents temporal averaging) of OEOF under different forcing frequencies are investigated first. The result is plotted in Figure 6. In the considered frequency range (i.e., 10 Hz to 3 kHz), the mean velocity is approximately constant at 0.8 mm/s. The variation of the mean velocity caused by OEOF in Figure 6 is below 0.1 mm/s (i.e., less than 13%).

Frequency Response of Oscillating Velocity. The frequency-independent mean velocity of OEOF in the considered frequency range provides us a solid foundation for measuring oscillating velocities, because the temporal resolution of LIFPA measurement on oscillating velocity relies on the mean flow velocity.[58]

Time series of oscillating velocities ($u' = u - U$) at four different forcing frequencies (f_f) are plotted in Figure 7a. The waveform of applied AC voltage is sinusoidal. Under low forcing frequencies (i.e., 10 and 50 Hz), the oscillating velocities precisely respond to the forcing frequencies, and

DOI: 10.1021/acs.analchem.7b02985
Anal. Chem. 2018, 90, 1652−1659

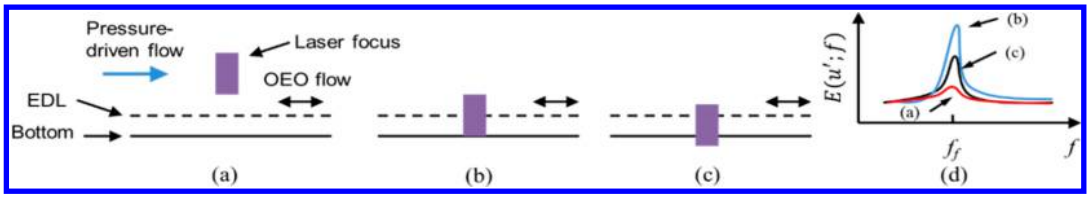

Figure 5. Relation between the position of laser focus and the peak intensity of velocity power spectrum $E(u';f)$, which is defined in eq 3. (a) The laser focus is away from the EDL. (b) the laser focus is located at the optimal position for measuring OEOF. (c) The laser focus has been moved out of the EDL. (d) The relations of the positions of laser focus with velocity power spectrum $E(u';f)$. Only at the position plotted in (b), the highest peak of $E(u';f)$ and maximum oscillating velocity can be achieved.

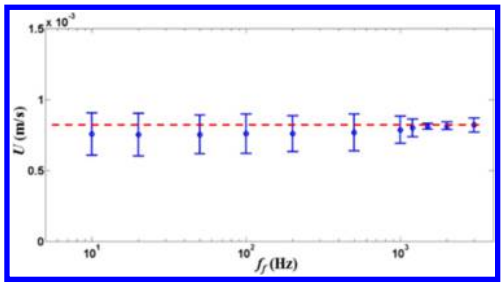

Figure 6. Mean velocity of flow under different forcing frequencies measured at a near wall position of z = 2 μm. The flow rate is Q = 2 μL/min. $E_A = 2 \times 10^3$ V/m. The red dashed line indicates the mean velocity (≈0.8 mm/s) of the unforced flow.

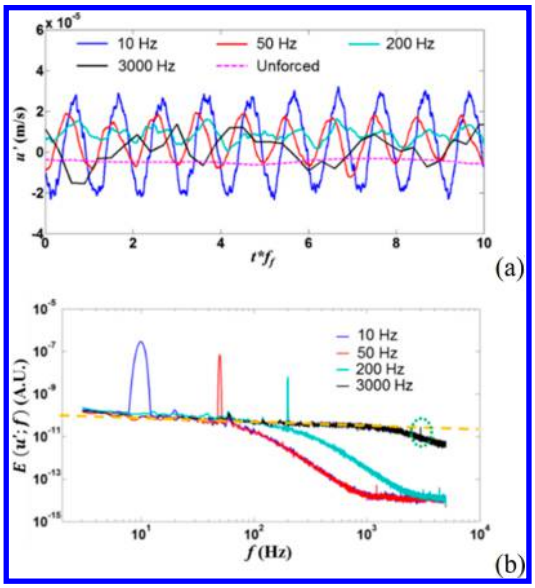

Figure 7. Time series and spectra of oscillating velocities in OEOF at z = 2 μm. The flow rate is Q = 2 μL/min. $E_A = 2 \times 10^3$ V/m. (a) Time series of original u' under four different AC signals, which are unforced, 10, 50, 200, and 3000 Hz, respectively. The applied waveforms are all sinusoidal. The time axis is normalized by f_f. (b) Power spectra of oscillating velocities of OEOF at near wall position. The yellow dashed line indicates the noise level of velocity signal in the unforced flow. The green dotted circle denotes the peak of velocity components at 3 kHz. The fast descending of $E(u';f)$ at the high frequency side of f_f is caused by the 12 dB low-pass filter of the current amplifier.

their waveforms are approximately sinusoidal. However, when the forcing frequency is increased to 200 Hz, the sinusoidal oscillating velocity cannot be easily distinguished from the time series. At 3 kHz, the signal looks completely random and no visible periodic signal can be distinguished, as plotted by the black line. Apparently, at this frequency, the contribution of noise to u' signal is very large.

The signal-noise relations can be more explicit from the power spectrum of u', i.e. $E(u';f)$, as shown in Figure 7b.

$$E(u';f) = \mathcal{F}(u')\cdot\overline{\mathcal{F}(u')} \quad (3)$$

where $\mathcal{F}(u')$ indicates the Fourier transform of u' and " ~ " represents complex conjugate.

In the figure, the yellow dashed line represents the noise level of u' at the same z positions in the unforced flow. It also indicates the noise level of LIFPA measurement. When f_f is 10, 50, and 200 Hz, the signal level is at least two orders higher than the noise level. The influence of noise is still tolerable. However, when forced at 3 kHz, the noise level could be larger than the signal peak at the forcing frequency. The high-frequency noise becomes dominant and velocity measurement becomes invalid at frequency higher than 3 kHz.

To remove the high frequency noise, relevant low-pass analog filters were used. At 10 and 50 Hz, a 12db low-pass analog filter with 100 Hz cutoff frequency (f_c) was applied. Due to large oscillating velocity and low noise after filtering, the measurement exhibited high signal-noise ratio (SNR). When f_f was increased to 200 Hz, a low-pass filter with f_c = 300 Hz had to be applied to suppress the analog noise from the detection system. For f_f = 3 kHz, the peak in the $E(u';f)$ was invisible until f_c = 3 kHz was applied. The SNR was significantly enhanced by the filter. The reason may be that shot noise, which increases with $f_c^{1/2}$, could be the main source of noise in fluorescence measurement.[59] Although the peak of $E(u';f)$ at 3 kHz can be attenuated by the low-pass analog filter, the shot noise is attenuated more since f_c is decreased from 10 kHz to 3 kHz. Therefore, decreasing f_c can reduce the noise and enhance the SNR of the LIFPA measurement.

Oscillating Velocity at Different f_f. The oscillating velocity can be further evaluated by $u_{rms} = \sqrt{\overline{u'^2_{de}}}$, where u'_{de} is the denoised oscillating velocity after numerically filtered by fast fourier transform (FFT). The bandwidth for bandpass FFT filter is 10 Hz (i.e., ± 5 Hz around the forcing frequency). The results are plotted in Figure 8.

At $E_A = 2 \times 10^3$ V/m and Q = 2 μL/min, the maximum detectable frequency response of the OEOF is up to 3 kHz. Beyond this frequency, even though a higher f_f is applied, the velocity signal of the OEOF is too weak to be distinguished from the noise.

As shown by the red dashed line, in the frequency range of 10−50 Hz, u_{rms} is approximately unchanged with f_f. This is qualitatively consistent with prediction by Wu et al.[47] While at $f_f \geq 100$ Hz, u_{rms} decreases with f_f, approximately by a power-law curve. The slope of the curve is around −0.66. To the best of our knowledge, this descending variation has never been

DOI: 10.1021/acs.analchem.7b02985
Anal. Chem. 2018, 90, 1652−1659

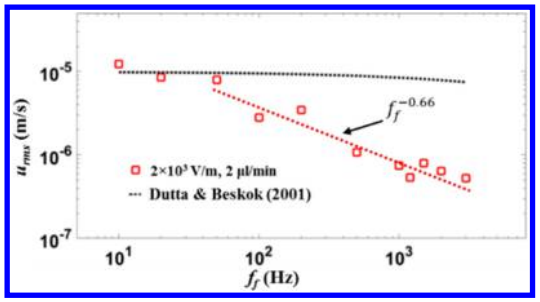

Figure 8. u_{rms} varies with f_f. The experimental data (red square) at z = 2 μm is compared with theoretical prediction (black dotted line) by Dutta and Beskok.[20] Note, the influence of the low-pass filter has been corrected as introduced in the main text.

reported before and is different from all the known theoretical works. As predicted by Dutta and Beskok,[20] the theoretical velocity of the OEOF can be expressed as

$$u_{theo}(\theta, \tilde{z}) = U_{HS}\mathrm{Im}\left\{2\Psi e^{i\theta}\sinh(\sqrt{i}\kappa\tilde{z}) + \frac{e^{i\theta}}{\sqrt{i}\kappa\alpha}\int_0^{\tilde{z}}\sinh[\sqrt{i}\kappa(\tilde{z}' - \tilde{z})]\sinh(\alpha\varphi^*)\mathrm{d}\tilde{z}'\right\} \quad (4)$$

where $U_{HS} = -\varepsilon\zeta E_A/\mu$ is the Helmholtz-Smoluchowski velocity related to E_A. $\zeta \approx -10$ mV is the ζ-potential and $\mu = 10^{-3}$ kg/ms is the dynamic viscosity of the fluid. It should be noted, since the bottom material is acrylic coated with a UV-transmission film, the exact ζ-potential is unknown. The ζ-potential adopted here is estimated from our experimental data at low frequency (<50 Hz). "Im" indicates imaginary part, $\theta = f_f t$ and $\tilde{z} = z/\lambda$ are the dimensionless time and spatial scales, respectively.$\tilde{z}' \in [0,\tilde{z}]$ is an alternative $\tilde{z}$ for integration only. $\kappa = \lambda/l_\nu$ is a dimensionless frequency quantity, where $l_\nu = (\nu/2\pi f_f)^{1/2}$ is the thickness of Stokes layer and $\nu = 10^{-6}$ m^2/s is the kinematic viscosity. $\alpha = \mathrm{eq}\zeta/k_BT$ is ionic energy parameter. Besides

$$\varphi^*(\tilde{z}') = \frac{4}{\alpha}\tanh^{-1}\left[\tanh\left(\frac{\alpha}{4}\right)e^{-\tilde{z}'}\right] \quad (5)$$

is the dimensionless electrostatic potential and

$$\Psi = \frac{1}{2\sqrt{i}\kappa\alpha\cosh(\sqrt{i}\kappa\tilde{z})}\left[\int_0^\infty \sinh[\sqrt{i}\kappa(\tilde{z}' - \tilde{z})]\sinh(\alpha\varphi^*)\mathrm{d}\tilde{z}'\right] \quad (6)$$

is a dimensionless function of $\tilde{z}$. In the considered frequency range (i.e., 10 Hz to 3 kHz), the corresponding l_ν is between 126.2 to 7.3 μm respectively and the corresponding κ is 7×10^{-5} to 1.19×10^{-3}. In this range, the theoretically predicated $u_{rms} = U_{HS}/\sqrt{2}$ decreases slowly with the increase of f_f, from nearly 10 μm/s to 7.5 μm/s, as plotted by the black dotted lines in Figure 8. In the plot of theoretical estimation, the influence of finite depth of focus has already been included on the result of Dutta and Beskok,[20] as

$$u_{rms,theo} = \sqrt{\int_0^1\left[\int_0^{10^{-6}/\lambda} u_{theo}(\theta, \tilde{z})\mathrm{d}\tilde{z}\right]^2\mathrm{d}\theta} \quad (7)$$

By comparing the experiment and theory, it can be seen when $f_f \leq 50$ Hz, the experimentally observed u_{rms} shows consistent results with the theoretical ones. However, while the forcing frequency is increased to 1 kHz, the difference between experiments and theory becomes more than 10 times.

Oscillating Velocity under Different Intensities of AC Electric Field. The effect of the intensity of AC electric fields E_A on the oscillating velocity u_{rms} was further investigated, as shown in Figure 9. Under f_f = 10, 50, and 200 Hz, with different

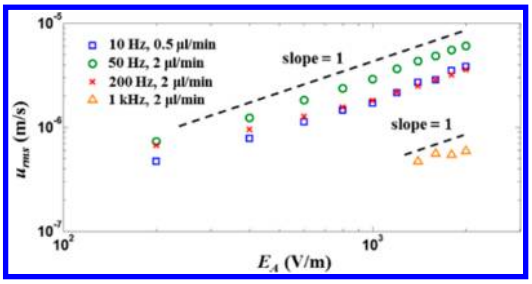

Figure 9. u_{rms} varies with applied electric field intensity at different f_f and Q at z = 2 μm. The dashed lines show the slope of power law curve. Note, the influence of low-pass filter has been corrected as discussed in the third section of the Discussion.

flow rate of 0.5 and 2 μL/min, the experimentally measured $u_{rms} - E_A$ plots all exhibit a slope of 1. This means u_{rms} has a linear relation with E_A. This observation is consistent with eq 4, where the oscillating velocities should be linearly proportional to E_A.[20] When the forcing frequency is increased to 1 kHz, due to the small oscillating velocities at low E_A, the velocity components related to 1 kHz is not distinguishable from the noise (i.e., the level of velocity signal is smaller than that of noise). Only when $E_A \geq 980$ V/m is the slope around 1 observed.

From Figure 9, it should be particularly noticed that u_{rms} under 10 Hz become much smaller than that under 50 Hz. This is because in this case, the flow rate of the pressure-driven bulk flow is only 0.5 μL/min. At 10 Hz, when the flow rate decreases from 2 μL/min to 0.5 μL/min, u_{rms} decreases from 12 μm/s to 4 μm/s. In other words, bulk flow velocity shows influence on the oscillating velocity of OEOF.

DISCUSSION

The discrepancy in the $u_{rms} \sim f_f$ relation between experiments and theory is crucial for nanoscopic physics and chemistry adjacent to interfaces. First, the discrepancy is not due to the potential saturation of LIFPA technique as discussed in the Appendix. Second, ICEOF is also not the cause of the discrepancy. In OEOF, when the electric field is applied, induced charges could cause variation of ζ on the electrodes' surfaces, as systematically studied by Squires and Bazant.[60] The microchannel can be analogous to an RC electric circuit, that is, resistor (the solution in microchannel) and capacitors (the fluids surround the electrodes) in serial. When the frequency of electric field is increased, even though the amplitude of external electric field intensity is fixed, the electric field intensity on the resistor and capacitor parts increases and decreases, respectively. Therefore, the ICEOF should result in the increase of u_{rms}, with increasing f_f. This is different from our observations in Figure 8. The influence of ICEOF could be excluded. This is also why the flow is named as OEOF, not ICEOF.

Since the model from Dutta and Beskok[20] relies on several assumptions, for example, constant ν, ζ, and electrostatic potential distribution in EDL, which are assumed to be

DOI: 10.1021/acs.analchem.7b02985
Anal. Chem. 2018, 90, 1652−1659

independent of E_A and f_f, any variations of these factors with forcing frequencies could cause the discrepancy between experiments and theories. For instance, if we assume ν increase with f_f or ζ decrease with f_f the discrepancy in the $u_{rms} \sim f_f$ curve between experiments and theory could be partially explained. Note, although in bulk fluids, Andrade and Dodd[61] found that when f_f was beyond a specific value, ν became decrease with increasing f_f, it is not clear if this relation can be applied to the OEOFs, where surface chemistry and physics becomes very important and complicated.

To qualitatively understand the influence of ν and ζ on the decay of the oscillating velocity, we approximate the OEOF as a 2D viscous oscillating plate flow. This is reasonable because the EDL is thin compared to the height of microchannel. The EOF is first developed in EDL near the channel wall and then diffuse from the wall toward channel center through viscous effects. The solution of such an oscillating plate flow can be assumed to be[62]

$$u' = kU_{HS}e^{-y\sqrt{\frac{f_f}{2\nu}}}\cos\left(f_f t - y\sqrt{\frac{f_f}{2\nu}}\right) \quad (8)$$

where k is a coefficient, which may not be a constant, but depends on ν and U_{HS}. For a given ν and y, from eq 8, one can see that u' (which is linearly related to u_{rms}) decreases with the increase of f_f when f_f is sufficiently large. If we assume ν increases with f_f or ζ decrease with f_f either one could lead to U_{HS} decrease with f_f. This might explain what we experimentally observed here.

Unfortunately, limited by the current experimental techniques, it is impossible to accurately measure ν, ζ, and electrostatic potential distribution in EDL, under the presence of AC electric fields. New measurement methods which are nonelectric and have nanoscale resolution are required to make the problem more clear.

CONCLUSION

In this investigation, the velocity of oscillating EOF is studied by LIFPA. The present work successfully shows the following: (1) The LIFPA system can detect up to 3 kHz velocity signal with high sensitivity. The smallest oscillating velocity that can be detected is around 600 nm/s. To the authors' knowledge, this is the first time that the oscillating velocity of OEOF can be determined experimentally up to 3 kHz. (2) u_{rms} decreases with f_f exponentially with a slope of −0.66, i.e. $u_{rms} \sim f_f^{-0.66}$. This result is different from the prediction based on models of Dutta and Beskok[20] and many other relevant works and cannot be explained by current theories. This might be caused by the change of viscosity with AC frequency. (3) In the investigated range of the electric field intensity, u_{rms} increases with E_A approximately under a linear relation, for the AC frequency up to 1 kHz.

The present study of the OEOF with LIFPA preliminarily shows there are new phenomena that have not been observed or predicted theoretically. However, measuring the velocity fluctuations alone cannot fully explain the abnormal OEOF velocity fluctuations. More efforts on measuring viscosity and local electric potential within EDL in microchannel under electric field are required in future investigations. This study is crucial on further understanding AC electrokinetic phenomena. It is also important for guiding the development of micro/nanoscale devices based on OEOF for various applications, especially for DNA and cell manipulation.

ASSOCIATED CONTENT

Supporting Information

The Supporting Information is available free of charge on the ACS Publications website at DOI: 10.1021/acs.analchem.7b02985.

Reliability of the LIFPA measurement, reliability of the AC voltages applied, and compensation for the low-pass filter (PDF)

AUTHOR INFORMATION

Corresponding Authors

*E-mail: ruiqiao@vt.edu.

*E-mail: guirenwang@sc.edu.

ORCID

Rui Qiao: 0000-0001-5219-5530

Guiren Wang: 0000-0002-5379-0814

Notes

The authors declare no competing financial interest.

ACKNOWLEDGMENTS

The work was supported by the U.S. National Science Foundation (No. CAREER CBET-0954977, MRI CBET-1040227, CBET-1336004) and the National Natural Science Foundation of China (No. 11672229), respectively.

REFERENCES

(1) Sphaier, L. A. *Int. Commun. Heat Mass Transfer* **2012**, *39*, 769−775.

(2) Kumar, V.; Paraschivoiu, M.; Nigam, K. D. P. *Chem. Eng. Sci.* **2011**, *66*, 1329−1373.

(3) Lee, C.-Y.; Chang, C.-L.; Wang, Y.-N.; Fu, L.-M. *Int. J. Mol. Sci.* **2011**, *12*, 3263−3287.

(4) Lin, B. *Microfluidics: Technologies and Applications*; Springer-Verlag: Berlin, Germany, 2011.

(5) Asadi, M.; Xie, G.; Sunden, B. *Int. J. Heat Mass Transfer* **2014**, *79*, 34−53.

(6) Green, N. G.; Ramos, A.; González, A.; Morgan, H.; Castellanos, A. *Phys. Rev. E: Stat. Phys., Plasmas, Fluids, Relat. Interdiscip. Top.* **2000**, *61*, 4011−4018.

(7) Studer, V.; Pépin, A.; Chen, Y.; Ajdari, A. *Analyst* **2004**, *129*, 944−949.

(8) Debesset, S.; Hayden, C. J.; Dalton, C.; Eijkel, J. C. T.; Manz, A. *Lab Chip* **2004**, *4*, 396−400.

(9) Gagnon, Z.; Chang, H.-C. *Electrophoresis* **2005**, *26*, 3725−3737.

(10) Ramos, A.; Morgan, H.; Green, N. G.; González, A.; Castellanos, A. *J. Appl. Phys.* **2005**, *97*, 084906.

(11) Bown, M. R.; Meinhart, C. D. *Microfluid. Nanofluid.* **2006**, *2*, 513−523.

(12) Ng, W. Y.; Goh, S.; Lam, Y. C.; Yang, C.; Rodríguez, I. *Lab Chip* **2009**, *9*, 802−809.

(13) Brown, A. B. D.; Smith, C. G.; Rennie, A. R. *Phys. Rev. E: Stat. Phys., Plasmas, Fluids, Relat. Interdiscip. Top.* **2000**, *63*, 016305.

(14) Gregersen, M. M.; Olesen, L. H.; Brask, A.; Hansen, M. F.; Bruus, H. *Phys. Rev. E* **2007**, *76*, 056305.

(15) Islam, N.; Reyna, J. *Electrophoresis* **2012**, *33*, 1191−1197.

(16) Ramos, A.; González, A.; Castellanos, A.; Green, N. G.; Morgan, H. *Phys. Rev. E: Stat. Phys., Plasmas, Fluids, Relat. Interdiscip. Top.* **2003**, *67*, 056302.

(17) Sasaki, N.; Kitamori, T.; Kim, H.-B. *Anal. Sci.* **2010**, *26*, 815−819.

(18) Urbanski, J. P.; Thorsen, T.; Levitan, J. A.; Bazant, M. Z. *Appl. Phys. Lett.* **2006**, *89*, 143508.

(19) González, A.; Ramos, A.; Green, N. G.; Castellanos, A.; Morgan, H. *Phys. Rev. E: Stat. Phys., Plasmas, Fluids, Relat. Interdiscip. Top.* **2000**, *61*, 4019−4028.

(20) Dutta, P.; Beskok, A. *Anal. Chem.* **2001**, *73*, 5097−5102.
(21) Kang, Y.; Yang, C.; Huang, X. *Int. J. Eng. Sci.* **2002**, *40*, 2203−2221.
(22) Yang, J.; Bhattacharyya, A.; Masliyah, J. H.; Kwok, D. Y. *J. Colloid Interface Sci.* **2003**, *261*, 21−31.
(23) Bhattacharyya, A.; Masliyah, J. H.; Yang, J. *J. Colloid Interface Sci.* **2003**, *261*, 12−20.
(24) Bazant, M. Z.; Ben, Y. *Lab Chip* **2006**, *6*, 1455−1461.
(25) Burch, D.; Bazant, M. Z. *Phys. Rev. E* **2008**, *77*, 055303.
(26) Olesen, L. H.; Bazant, M. Z.; Bruus, H. *Phys. Rev. E* **2010**, *82*, 011501.
(27) Aboelkassem, Y. *Comput. Fluids* **2011**, *52*, 104−115.
(28) Liu, Q.; Jian, Y.; Yang, L. *Phys. Fluids* **2011**, *23*, 102001.
(29) Afonso, A. M.; Alves, M. A.; Pinho, F. T. *J. Eng. Math.* **2011**, *71*, 15−30.
(30) Sousa, J. J.; Afonso, A. M.; Pinho, F. T.; Alves, M. A. *Microfluid. Nanofluid.* **2011**, *10*, 107−122.
(31) Jian, Y.-j.; Liu, Q.-s.; Yang, L.-g. *J. Non-Newtonian Fluid Mech.* **2011**, *166*, 1304−1314.
(32) Moghadam, A. J. *Eur. J. Mech. B-Fluid* **2014**, *48*, 1−12.
(33) Lin, T.-Y.; Chen, C.-L. *Appl. Math. Model* **2013**, *37*, 2816−2829.
(34) Reppert, P. M.; Morgan, F. D. *J. Colloid Interface Sci.* **2002**, *254*, 372−383.
(35) Erickson, D.; Li, D. *Langmuir* **2003**, *19*, 5421−5430.
(36) Moghadam, A. J. *Eur. J. Mech. B-Fluid* **2012**, *34*, 91−96.
(37) Joekar-Niasar, V.; Schotting, R.; Leijnse, A. *Computat. Geosci.* **2013**, *17*, 497−513.
(38) Scott, M.; Kaler, K. V. I. S.; Paul, R. *J. Colloid Interface Sci.* **2001**, *238* (238), 449−451.
(39) Suh, Y. K.; Kang, S. *Phys. Rev. E* **2009**, *79*, 046309.
(40) Storey, B. D.; Edwards, L. R.; Kilic, M. S.; Bazant, M. Z. *Phys. Rev. E* **2008**, *77*, 036317.
(41) Wang, S.; Zhao, M. *Bound. Value Probl.* **2014**, *2014*, 215.
(42) Hrdlička, J.; Patel, N. S.; Šnita, D. *Electrophoresis* **2014**, *35*, 1790−1794.
(43) Bazant, M. Z.; Kilic, M. S.; Storey, B.; Ajdari, A. *Adv. Colloid Interface Sci.* **2009**, *152*, 48−88.
(44) Levitan, J. A.; Devasenathipathy, S.; Studer, V.; Ben, Y.; Thorsen, T.; Squires, T. M.; Bazant, M. Z. *Colloids Surf., A* **2005**, *267*, 122−132.
(45) Minor, M.; van der Linde, A. J.; van Leeuwen, H. P.; Lyklema, J. *J. Colloid Interface Sci.* **1997**, *189*, 370−375.
(46) Sadr, R.; Hohenegger, C.; Li, H.; Mucha, P. J.; Yoda, M. *J. Fluid Mech.* **2007**, *577*, 443−456.
(47) Wu, W.-I.; Ewing, D.; Ching, C. Y.; Selvaganapathy, P. R. *Microfluid. Nanofluid.* **2013**, *15*, 127−135.
(48) Kneller, A. R.; Haywood, D. G.; Jacobson, S. C. *Anal. Chem.* **2016**, *88*, 6390.
(49) Wang, G.; Yang, F.; Zhao, W. *Lab Chip* **2014**, *14*, 1452−1458.
(50) Wang, G.; Yang, F.; Zhao, W. *Phys. Rev. E: Stat. Phys., Plasmas, Fluids, Relat. Interdiscip. Top.* **2016**, *93*, 013106.
(51) Wang, G.; Yang, F.; Zhao, W.; Chen, C.-P. *Lab Chip* **2016**, *16*, 1030−1038.
(52) Wang, G. R. *Lab Chip* **2005**, *5*, 450−456.
(53) Zhao, W.; Yang, F.; Khan, J.; Reifsnider, K.; Wang, G. *Exp. Fluids* **2016**, *57*, 1−12.
(54) Kuang, C.; Qiao, R.; Wang, G. *Microfluid. Nanofluid.* **2011**, *11*, 353−358.
(55) Yang, F.; Yang, X.; Jiang, H.; Bulkhaults, P.; Wood, P.; Hrushesky, W.; Wang, G. *Biomicrofluidics* **2010**, *4*, 013204.
(56) Bruus, H. *Theoretical Microfluidics*; Oxford University Press: Oxford, U.K., 2008.
(57) Mortensen, N. A.; Okkels, F.; Bruus, H. *Phys. Rev. E* **2005**, *71*, 057301.
(58) Zhao, W.; Yang, F.; Khan, J.; Reifsnider, K.; Wang, G. *Exp. Fluids* **2015**, *56*, 39.
(59) Wang, G. R.; Fiedler, H. E. *Exp. Fluids* **2000**, *29*, 265−274.
(60) Squires, T. M.; Bazant, M. Z. *J. Fluid Mech.* **1999**, *509*, 217−252.
(61) da C. Andrade, E. N.; Dodd, C. *Proc. R. Soc. London, Ser. A* **1946**, *187*, 296−337.
(62) White, F. *Viscous Fluid Flow*; McGraw-Hill, Inc: New York, 1991.

DOI: 10.1021/acs.analchem.7b02985
Anal. Chem. 2018, 90, 1652−1659